ACS Photonics

Article

pubs.acs.org/journal/apchd5

Emission Quenching of Magnetic Dipole Transitions near a Metal Nanoparticle

Dmitry N. Chigrin,* Deepu Kumar, David Cuma, and Gero von Plessen

Institute of Physics (1A), RWTH Aachen University, 52056 Aachen, Germany

Supporting Information

ABSTRACT: The emission quenching of magnetic dipole transitions due to electromagnetic coupling to a metal nanoparticle is studied theoretically. We show that, at nanometer distances to the nanoparticle surface, the quenching is much weaker than that of electric dipole transitions, resulting in far higher radiative quantum efficiencies. This difference is explained by the fact that the electric field induced by an oscillating magnetic dipole and responsible for the energy transfer to the metal has a weaker distance dependence than the electric field of an electric dipole. Our results imply that magnetic dipole transitions may be superior to electric ones if coupling to a metallic nanoantenna over sub-10 nm distances is used to enhance optical emission from a quantum emitter.

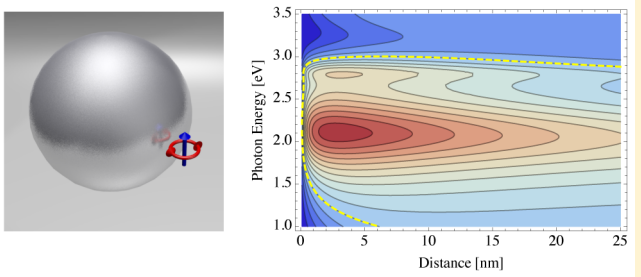

KEYWORDS: *nanoplasmonics, light−matter interactions, magnetic dipole transitions, local and nonlocal response*

In metal nanoparticles, collective electron excitations known as particle-plasmon polaritons can be excited by light. They show themselves as resonances in the optical response of the nanoparticles.[1] Particle-plasmon polaritons have been studied extensively due to their versatile spectral behavior and the intriguing optical near-field phenomena associated with the resonances. In particular, they give rise to optical near-field enhancement near the nanoparticle surface, a phenomenon that is involved in a number of optical effects such as surface-enhanced Raman scattering (SERS) and surface-enhanced infrared absorption (SEIRA).[2,3] In addition, the nanostructuring of near-fields allows one to manipulate optical selection rules.[4]

Another important near-field phenomenon associated with particle-plasmon polaritons is the emission enhancement of atomic, ionic, molecular, and quantum-dot emitters coupled to a metallic nanoparticle. The optical near-field of the emitter excites particle-plasmon polaritons in the nanoparticle. If the excitation conditions are such that the combined dipole moment of the coupled system is higher than that of the emitter alone, the radiative lifetime of the emitter is shortened and the emission rate is enhanced; the particle then acts as a nanoantenna. If the emission process competes with nonradiative loss processes in the emitter, this enhancement tends to improve the radiative quantum efficiency of the emitter, defined as the ratio of the number of photons emitted to the number of photons absorbed.[5] The improved radiative quantum efficiency is applied, for example, in the surface-enhanced fluorescence (SEF) technique.[6] However, the near-field of the emitter also drives electrical surface currents in the nanoparticle so that a fraction of the oscillation energy is lost to nonradiative relaxation processes in the metal. At small distances between emitter and nanoparticle (on the order of a few nanometers), this fraction even becomes dominant so that the radiative quantum efficiency decreases substantially, an effect known as emission quenching.[7−11] A number of theoretical and experimental studies have investigated emission quenching and its dependence on the distance between emitter and nanoparticle surface.[7,10−22] Emission quenching plays a useful role in photoluminescence quenching assays employing bioconjugated metal nanoparticles as energy transfer acceptors for applications in the life sciences (ref 23 and references therein). In contrast, emission quenching detrimentally limits the applicability of metallic nanoparticles when they are used as nanoantennas for emitters placed in the direct vicinity of the nanoparticle surface, for example, to enhance fluorescence.

Light emission processes and quenching near a metallic nanostructure are typically studied within the electric dipole (ED) approximation.[24] However, there are important classes of emitters such as quantum dots[25,26] or rare earth ions[27,28] for which one has to go beyond the electric dipole approximation in order to give adequate descriptions. In such cases, a finite size of the emitter[25,26] or higher order multipole transitions[29] have to be taken into account. In particular, magnetic-dipole (MD) transitions have recently attracted a lot of interest. For example, many transitions in rare-earth ions, for example, the $^4I_{13/2} \rightarrow {}^4I_{15/2}$ transition in Er^{3+} ions, have considerable MD contributions.[27,28] The recent interest in MD transitions is motivated by the realization that they can have appreciable strengths and offer excellent probes into the magnetic part of

Received: July 21, 2015
Published: December 3, 2015

DOI: 10.1021/acsphotonics.5b00397
ACS Photonics 2016, 3, 27−34

the local optical density of states, which can be of particular importance in the field of metamaterials.

Recent studies of the MD emission modification near metallic nanoparticles have mainly focused on relatively large emitter-nanoparticle separations,[30−34] where the inevitable ohmic losses originating from nonradiative relaxation processes in the metal do not dominate the near-field response of the nanoparticle. For MD transitions, little is known about emission quenching caused by coupling to metal nanoparticles over very small distances. In the present paper, we analyze this effect by calculating the optical emission from MD and ED emitters coupled to a metal nanoparticle. We demonstrate that the reduction in radiative quantum efficiency that is caused by nonradiative relaxation in the metal is, near the nanoparticle surface, much smaller for MD than for ED transitions. This difference is explained by the fact that the distance dependence of the electric field induced by the magnetic dipole is weaker than that of the electric near-field of the electric dipole. Our results imply that MD transitions may be superior to ED ones when coupling to a metallic nanoantenna over sub-10 nm distances is used to enhance optical emission from a quantum emitter.

In what follows, we consider a point dipole emitter (electric or magnetic) placed at a distance d from the surface of a metal sphere of radius a (Figure 1). The metal chosen here is silver,

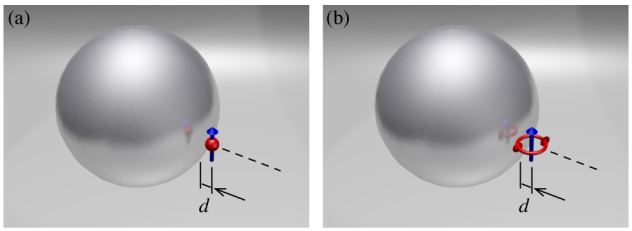

Figure 1. Sketches of point electric (a) and magnetic (b) dipoles placed at a distance d from the surface of a silver sphere with radius a. Both the silver sphere and dipoles are placed in a host medium with a refractive index n_b = 1.5. The dipoles can have an arbitrary orientation with respect to the surface. The dipoles are shown not to scale.

but may also be another material with good plasmonic properties, for example, doped $Cu_{2-x}S$.[35,36] The dielectric function of silver, ε, is described using the local[37] and nonlocal[38] Lorentz−Drude models (see Supporting Information (SI) for more details). The refractive index of the host medium, n_b, is set to that of glass ($n_b = \sqrt{\varepsilon_b} = 1.5$) to represent an experimentally valid situation. Here ε_b is the dielectric constant of the host medium. Emission from a point dipole in the presence of a metallic sphere is described within the Mie formalism.[39] In this formalism, the radiative decay rate is determined by the total radiated power calculated as an integral of the Poynting vector over a full solid angle in the far-field.[40] The nonradiative decay rate is given by the energy dissipation rate associated with the current induced in the particle by the electric field of the dipole.[40] The radiative ($\gamma^{R}_{e,\parallel}$, $\gamma^{R}_{e,\perp}$) and nonradiative ($\gamma^{NR}_{e,\parallel}$, $\gamma^{NR}_{e,\perp}$) decay rates of the point electric dipole in the presence of a nanoparticle have been presented in ref 40 and are summarized in the SI. Here the index e(m) is for electric(magnetic) transitions. We distinguish between parallel (∥) and perpendicular (⊥) orientations of the dipole with respect to the sphere surface. For the MD transitions, expressions for the total ($\gamma_{m,\parallel}$, $\gamma_{m,\perp}$) and radiative ($\gamma^{R}_{m,\parallel}$, $\gamma^{R}_{m,\perp}$) decay rates have recently been reported in refs 31,41, and 42. Here we derive explicit expressions for the nonradiative ($\gamma^{NR}_{m,\parallel}$, $\gamma^{NR}_{m,\perp}$) decay rate of the MD transition following an approach presented in ref 43; see SI for details. Each decay rate is normalized with respect to the radiative decay rate in the absence of the nanoparticle. With this normalization, classical approaches such as that presented here deliver equivalent results to those of a quantum optical description.[44] To describe the emission modification for an ensemble of atoms or ions, whose transitions dipole moments are randomly oriented, the decay rates need to be averaged over all possible dipole orientations. This can be done by averaging the rates for the parallel and perpendicular dipole orientations with weight factors of two and one, respectively, $\gamma^{R(NR)}_{e(m)} = (2\gamma^{R(NR)}_{e(m),\parallel} + \gamma^{R(NR)}_{e(m),\perp})/3$.[9]

As an example of results obtained from the calculations, the black solid lines in Figure 2a and b, respectively, show the

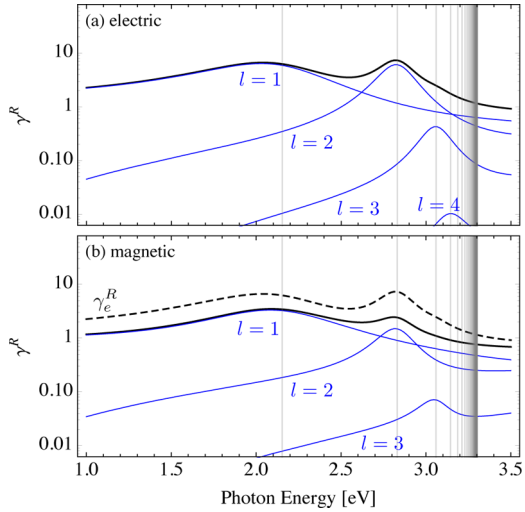

Figure 2. Radiative rate (black solid line) of electric (a) and magnetic (b) dipoles placed 10 nm from the surface of a silver sphere with radius a = 50 nm vs photon energy of the dipole transition. The contributions of individual multipole orders (l = 1, 2, 3, ...) to the total rate are depicted as thin blue lines. In the bottom panel (b), the radiative rate of an electric dipole (black dashed like) is duplicated to facilitate comparison. All rates have been normalized to those of the nanoparticle-free ones and are averaged over the dipole orientation with respect to the sphere surface. Vertical gray lines correspond to PPP resonance frequencies.

orientation-averaged radiative decay rates, γ^{R}_{e} and γ^{R}_{m}, of electric and magnetic dipoles placed at a distance d = 10 nm from the surface of a silver nanosphere with radius a = 50 nm. All rates have been normalized to the radiative decay rate of the dipole in the nanoparticle-free host medium. Both in the case of ED and MD transitions, the dependence of the radiative decay rate on the photon energy of the emission exhibits several resonances. The spectral positions of these resonances correspond to poles of the Mie coefficients (vertical gray lines) and are associated with excitations of particle-plasmon-polaritons (PPPs) of different electric multipole orders in the silver nanosphere.[40] Contributions from individual multipole orders (l = 1, 2, 3, ...) to the total rate are depicted as thin blue lines. Only low-order multipoles contribute considerably to the radiative decay rate. Higher-order multipoles do not contribute appreciably to the radiative decay due to their predominantly dissipative nature.[9] Their frequencies converge to the surface plasma frequency of the flat silver surface, $\hbar\omega$ = 3.31 eV.

DOI: 10.1021/acsphotonics.5b00397
ACS Photonics 2016, 3, 27−34

Resonances associated with the magnetic multipoles of the nanosphere are known to exist in the spectral range where the permittivity of silver is positive,[45] that is, $\hbar\omega > 5.4$ eV. In the spectral range where silver demonstrates a metallic behavior ($\hbar\omega < 3.83$ eV), the contribution of the magnetic multipoles is negligible[45] and the emission decay of the magnetic transition is predominantly caused by the coupling of the electric field induced by the magnetic dipole to the electric multipoles of the nanosphere. For this reason, the radiative decay rate of the magnetic transition essentially follows the spectral profile of that of the electric one. The absolute value of the magnetic radiative decay rates, however, is two to three times smaller.

The difference is larger in the case of the nonradiative processes. In this case, all higher-order PPPs contribute to the energy dissipation.[9,43] In Figure 3, the nonradiative decay rates,

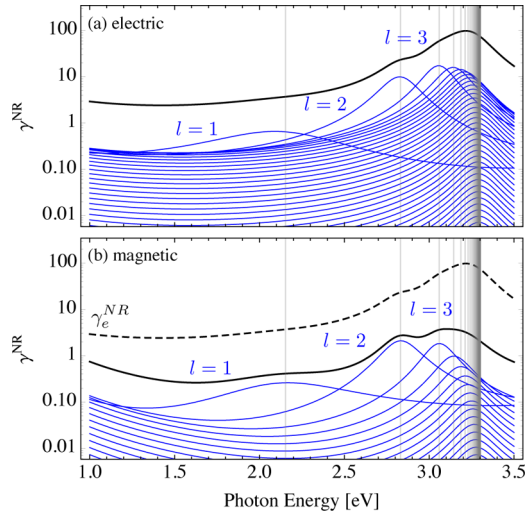

Figure 3. Nonradiative rate (black solid line) of electric (a) and magnetic (b) dipoles placed 10 nm away from the surface of a silver sphere with radius a = 50 nm. The contributions of individual multipole orders (l = 1, 2, 3, ...) to the total rate are depicted as thin blue lines. In the bottom panel (b) the nonradiative rate of an electric dipole (black dashed like) is duplicated to simplify comparison. All rates have been normalized to those of the nanoparticle-free ones and are averaged over the dipole orientation with respect to the sphere surface. Vertical gray lines correspond to PPP resonance frequencies.

γ_e^{NR} and γ_m^{NR}, (black solid lines) are shown for electric (a) and magnetic (b) dipole transitions of a dipole placed at the distance d = 10 nm from the surface of the nanosphere with radius a = 50 nm. Contributions of individual multipole orders to the total rate are depicted as thin blue lines. All rates have been normalized to the radiative decay rate of the dipole in the nanoparticle-free host medium. One can see that both for the electric and magnetic dipoles a contribution from the higher-order multipoles is not negligible even at the frequency of the first (l = 1) PPP resonance. Because the resonance frequencies of the higher-order PPPs converge to the surface plasma frequency of the flat silver surface, the nonradiative decay rate shows a peak near this frequency. Similar to the case of the radiative processes, the normalized nonradiative rate spectrum of the magnetic transition follows the spectrum of the electric one, remaining at the same time up to ten times smaller in absolute value.

While Figures 2 and 3 compare the spectral dependencies of the decay rates for ED and MD transitions, the following section studies the quantitative differences between the decay rates at selected frequencies. These differences depend on the distance of the emitter to the nanoparticle surface. In Figure 4,

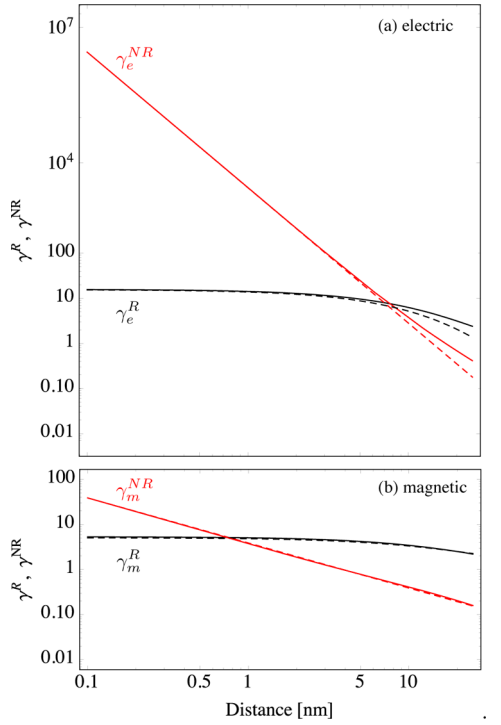

Figure 4. Normalized orientation averaged radiative (black lines) and nonradiative (red lines) decay rates versus distance to the nanoparticle surface in the near-field regime for electric (a) and magnetic (b) dipoles at the first (l = 1) PPP resonance frequency. Solid lines correspond to rigorous Mie calculations. Dashed lines depict quasi-static approximations eqs 1−4.

the radiative and nonradiative decay rates at the frequency of the first (l = 1) PPP resonance of the silver sphere with radius a = 50 nm are shown as functions of the distance to the nanoparticle surface. The solid lines have been calculated using the rigorous Mie formalism. A comparison between Figure 4a and b shows that the nonradiative decay rate of the MD transition is much lower than that of the electric one in the distance range studied here. This difference is a factor of 10 at a distance of 10 nm (as already shown in Figure 3) and becomes much larger at smaller distances. In contrast, the radiative decay rate of the MD transition lies only a factor of approximately 2 below that of the electric one over the whole distance range shown in Figure 4.

To understand why the nonradiative decay rates of ED and MD transitions show such different distance dependencies, we compare them in the quasi-static regime, that is, for the dipole positioned in close proximity to the nanosphere surface and $k_b a \ll 1$. Here k_b is the wavenumber in the host medium. In the near-field regime, the following form of the nonradiative rate of the electric dipole placed at a distance d from the nanosphere surface is obtained[43]

$$\gamma_e^{NR} \sim \frac{1}{4}\mathrm{Im}\left[\frac{(\varepsilon - \varepsilon_b)}{(\varepsilon + \varepsilon_b)}\right]\frac{1}{k_b^3}\frac{1}{d^3} \quad (1)$$

where d is the distance between the dipole and the sphere surface. This asymptotic expression is plotted as a dashed red

DOI: 10.1021/acsphotonics.5b00397
ACS Photonics 2016, 3, 27−34

line in Figure 4a. It shows an excellent agreement with the result of the rigorous Mie calculation (red solid line). Equation 1 reproduces the $1/d^3$ distance dependence of the nonradiative decay rate near a flat metal surface.[29,46,47] In the case of a flat surface, the usual $1/d^3$ distance dependence of the electric field produced by an electric dipole results in an energy dissipated in the metal that is proportional to $1/d^6$, which after integration over the metallic half space yields the $1/d^3$ behavior.[46] The agreement of the asymptotic eq 1 with the distance dependence for the flat metal surface means that the precise curvature of the metal has little effect on the distance dependence if the electric dipole is close enough to the surface. For the MD transition coupled to a nanosphere, we obtain in the quasi-static limit, following a similar approach as ref 43 (see SI for more details):

$$\gamma_m^{NR} \sim \frac{1}{4}\mathrm{Im}\left[\frac{(\varepsilon-\varepsilon_b)}{(\varepsilon+\varepsilon_b)}+\frac{(\varepsilon-\varepsilon_b)}{2\varepsilon_b}\right]\frac{1}{k_b}\frac{1}{d} \tag{2}$$

This expression is plotted as a dashed red line in Figure 4b. Again, it shows an excellent agreement with the result of a rigorous Mie calculation (red solid line). Note that in eq 2, the first term coincides with the quasi-static expression for the nonradiative decay rate of a magnetic dipole near a flat metal surface;[29,46,47] the second term in eq 2 is a residual contribution from coupling to the magnetic multipoles of the nanosphere and, in contrast to the first term, has a nonresonant character. In the case of the flat surface, the asymptotic $1/d$ distance dependence is a result of the $1/d^2$ distance dependence of the electric field induced by the oscillating magnetic dipole; the energy dissipated in the metal is then proportional to $1/d^4$, resulting, after integration over the metallic half space, in the $1/d$ behavior known from the literature.[46] The similarity of the first term in eq 2 to the quasi-static expression for the nonradiative decay rate near a flat surface suggests that the same explanation for the $1/d$ dependence holds in the case of the spherical surface. We conclude that the vast difference between the distance dependencies of the nonradiative decay rates of ED and MD transitions can be traced back to the difference between the $1/d^3$ distance dependence of the electric field produced by an electric dipole and the $1/d^2$ distance dependence of the electric field induced by the oscillating magnetic dipole.

As shown by the black solid lines in Figure 4, the radiative decay rates appear to exhibit much more gradual distance dependencies than the nonradiative ones. The reason for this difference becomes obvious when we consider again the quasi-static limit of the rigorous Mie treatment. In this limit, we obtain for the orientation-averaged radiative decay rate of the ED transition[43]

$$\gamma_e^R \approx \left|2a^3\left(\frac{\varepsilon-\varepsilon_b}{\varepsilon+2\varepsilon_b}\right)\right|^2\frac{1}{\rho^6} \sim |\alpha_1|^2\frac{1}{\rho^6} \tag{3}$$

and for that of the MD transition (see SI for details)

$$\gamma_m^R \approx \frac{1}{4}k_b^2\left|a\rho^2+2a^3\left(\frac{\varepsilon-\varepsilon_b}{\varepsilon+2\varepsilon_b}\right)\right|^2\frac{1}{\rho^4}+1 \sim |\alpha_1|^2\frac{1}{\rho^4} \tag{4}$$

where $\rho = a + d$ is the distance between the dipole and the sphere center, and $\alpha_1 = a^3(\varepsilon-\varepsilon_b)/(\varepsilon+2\varepsilon_b)$ is the quasi-static dipole polarizability of a sphere.[1,24] Equations 3 and 4 are plotted as dashed black lines in Figure 4. They show an excellent agreement with the results of the rigorous Mie calculation (black solid lines). The asymptotic power dependencies in eqs 3 and 4 can be understood within the dipole approximation. In this approximation, the radiative decay rate of a point dipole, $\gamma_{e(m)}^R$, is proportional to the absolute square of the dipole moment, $\vec{\mu}$, induced in the nanoparticle by the external electric field, $\mathbf{E}$.[24] In the quasi-static limit, the induced dipole moment is given by $\vec{\mu} = \alpha_1\mathbf{E}$, where α_1 is the quasi-static dipole polarizability of the nanoparticle. Here, a radiative correction to the polarizability is neglected for simplicity. In the near-field zone, where the emission quenching phenomena become important, the electric fields generated by the electric and magnetic dipoles scale with distance between the radiating dipole and the center of the nanoparticle, ρ, as $|\mathbf{E}| \sim 1/\rho^3$ and $|\mathbf{E}| \sim 1/\rho^2$, respectively.[24] As a result, the normalized radiative decay rates of ED and MD transitions are asymptotically proportional to $\gamma_e^R \sim |\alpha_1|^2/\rho^6$ and $\gamma_m^R \sim |\alpha_1|^2/\rho^4$, respectively. Thus, the dependencies of γ_e^R and γ_m^R on ρ are steeper than those of γ_e^{NR} and γ_m^{NR} on d. However, since even a small value of the distance d between emitter and nanoparticle surface means a relatively large value of $\rho = a + d$, the dependencies of the radiative decay rates on d appear much more gradual in the double-logarithmic plots of Figure 4 than those of the nonradiative decay rates.

The differences between the decay rates of electric and magnetic transitions near a metal nanoparticle lead to dramatic differences between their radiative quantum efficiencies. The radiative quantum efficiency of a transition is defined as the number of emitted photons per absorbed photon. In the following, the terms "extrinsic/intrinsic quantum efficiency" refer to the radiative quantum efficiency of the transition in the presence/absence of a metal nanoparticle, respectively. The extrinsic quantum efficiency, η, is related to the intrinsic one, η_0, through[8]

$$\eta = \frac{\gamma^R}{\gamma^R+\gamma^{NR}+(1-\eta_0)/\eta_0} \tag{5}$$

Here the radiative γ^R and nonradiative γ^{NR} rates are normalized to the radiative decay rate in the absence of the nanoparticle. The intrinsic quantum efficiency η_0 accounts for all intrinsic nonradiative transitions in the emitter in the absence of the nanoparticle. Figure 5 shows η as a function of the distance to the nanoparticle surface at the frequency of the first ($l = 1$) PPP resonance. Here the intrinsic quantum efficiency η_0 is assumed to be 100%. Far away from the nanosphere surface, the

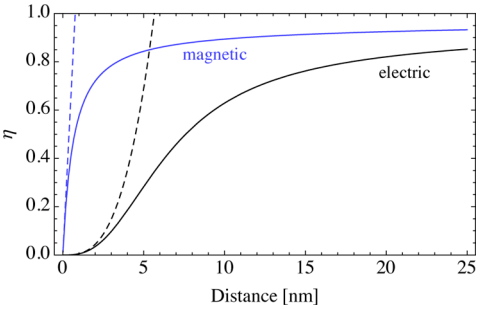

Figure 5. Orientation averaged extrinsic quantum efficiency of electric (solid black line) and magnetic (solid blue line) dipole at the first ($l = 1$) PPP resonance frequency. The intrinsic quantum efficiency is assumed to be 100% for both electric and magnetic dipole transitions. Dashed lines depict the asymptotic quasi-static limit of the extrinsic quantum efficiency.

DOI: 10.1021/acsphotonics.5b00397
ACS Photonics 2016, 3, 27−34

influence of the particle can be neglected and the extrinsic quantum efficiency η approaches 1. Near the nanoparticle surface, the nonradiative processes in the metal become dominant, resulting in a strong reduction of η. It is important to note that the extrinsic quantum efficiency of the MD transition remains relatively large even very close to the particle surface. For example, at a distance of d = 1 nm between dipole and nanosphere surface, the extrinsic quantum efficiency of the MD transition is 58%, while the extrinsic quantum efficiency of the ED transition is effectively zero (0.5%). In other words, the MD transitions experience strong emission quenching only in a much narrower zone around the nanoparticle than the ED transitions. This striking difference is a main result of the present Letter. It is a consequence of the distance dependencies of the decay rates discussed in the context of eqs 1−4 and Figure 4: (i) with decreasing distance d, the nonradiative decay rate of the MD transitions grows much more slowly ($\sim 1/d$) than the nonradiative rate of the ED transitions ($\sim 1/d^3$), resulting in much smaller absolute values of the nonradiative decay rate at the same distance, for example, d = 1 nm; and (ii) the radiative decay rates of magnetic and electric transitions are both almost independent of d at distances below 10 nm. For comparison, Figure 5 also shows the asymptotic quasi-static limits of the extrinsic quantum efficiency, which have been calculated from eqs 1−4 (dashed lines).

In contrast to the case η_0 = 1 shown in Figure 5, a transition with poor intrinsic quantum efficiency can experience an enhancement of the radiative quantum efficiency when coupled to a metal nanoparticle. It is interesting to ask what effects the differences between ED and MD transitions discussed above have on this radiative enhancement. In Figure 6, the enhancement of the extrinsic quantum efficiency of electric (a) and magnetic (b) dipole transitions is shown in a two-dimensional map for the case of an intrinsic quantum efficiency of 10%, which is a reasonable value for a transition in embedded rare-earth ions with poor η_0.[48] The radius of the silver sphere is a = 50 nm. The yellow dashed line corresponds to the case of the extrinsic quantum efficiency matching the intrinsic one and separates regions of reduced and enhanced quantum efficiency. Emission is enhanced near the first and second PPP resonances of the nanosphere. The maximal enhancement is comparable for the ED and MD transitions, being 3.3 and 3.1 times, respectively. Near the nanosphere surface, however, the ED and MD transitions behave very differently. The emission from electric dipoles placed closer than 3 nm to the sphere surface is strongly suppressed (quenched). In contrast, the emission from the magnetic dipole remains enhanced as close as 1 nm to the nanosphere surface. Thus, our earlier observation from Figure 4 that the emission quenching of MD transitions is restricted to a much narrower zone around the nanoparticle than that of ED transitions applies also to the case of poor intrinsic quantum efficiency. In addition to the short-distance quenching at the first and second PPP resonances, emission is also suppressed above 2.9 eV at all distances for both ED and MD transitions. This is a consequence of the low radiative and high nonradiative decay rates of the higher order PPP resonances beyond l = 2 (cf. Figures 2 and 3).

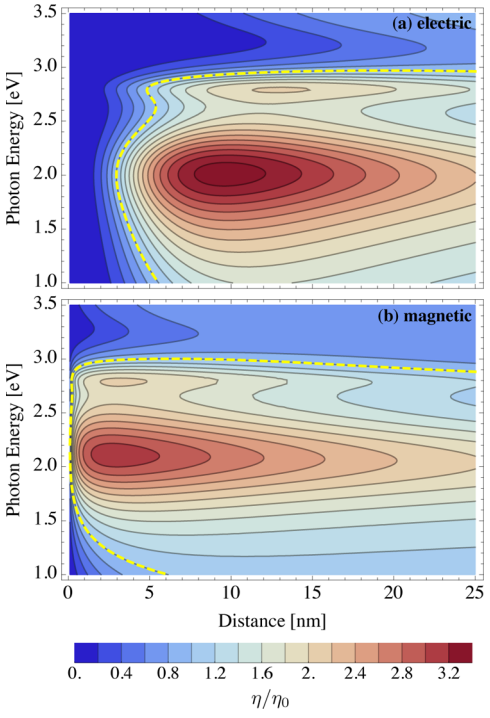

Figure 6. Enhancement of extrinsic quantum efficiency of electric (a) and magnetic (b) dipole transitions averaged over dipole orientation. The intrinsic quantum efficiency is assumed to be 10% for both electric and magnetic dipoles. The yellow dashed lines correspond to the case of the extrinsic quantum efficiency matching the intrinsic one and separate regions of suppressed and enhanced quantum efficiency.

At a few nanometers distance between emitting dipole and the nanoparticle surface, the induced currents are strongly localized in space and show large gradients on the length scale of a fraction of nanometer. In this situation, the nonlocality of the electromagnetic response of the metal may become important in the correct description of the light-matter interaction.[10,38,49−52] We have assessed the influence of the nonlocality on the emission quenching in this distance regime and shown (see SI for details) that at short distances to the particle surface the nonlocality leads to slightly lower extrinsic quantum efficiencies. The reduction of η is caused by the additional electronic dissipation known to occur in finite-size metal nanoparticles.[38] The main effect of the reduction is that the zone in which quenching dominates the ED transition at the l = 1 resonance frequency of the nanosphere widens by ∼1 nm, while the extrinsic quantum efficiencies of both ED and MD transition remains almost unchanged at frequencies of the higher order resonances of the nanosphere. At the same time, MD transitions stay superior to ED ones over the entire range of distances.

Above we have treated the emitter as a point dipole. This approximation is no longer valid when d approaches the dimension of the emitter, that is, ∼0.1 nm in the case of rare-earth ions. Then the finite dimension of the emitter has to be considered. Moreover, our approach ceases to apply at distances below ∼0.2 nm also because in this distance range the Mie formalism begins to break down due to the failure of the classical boundary conditions between two homogeneous media.[50] The corresponding spatial variation of the electric field takes place on length scales smaller than 0.1 nm, which is smaller than the interatomic distance of silver (about 0.29 nm). Furthermore, quantum effects begin to become important at such distances.[53−55] Spill-out of electron density outside the metal surface, electron tunneling from the emitter into a metallic nanoparticle and other effects could further modify the distance dependence of the emission quenching. To treat these

DOI: 10.1021/acsphotonics.5b00397
ACS Photonics 2016, 3, 27−34

effects, a first-principles quantum-mechanical description would be necessary. However, the development of such a description for the large nanoparticles considered here would go beyond the scope of the present work.

While no statement is possible below ∼0.2 nm, our results demonstrate that in the distance range beyond ∼0.2 nm, the reduced quenching of MD transitions predicted here should be large enough as to be experimentally demonstrable. As shown in Figures 5 and 6, the spatial range in which quenching is dominant is expected to have an extension of less than 1 nm for MD transitions, while it is several nanometers for ED transitions. Further calculations (see SI for further details) have demonstrated that this drastic difference also appears for oblate spheroids; we therefore expect it to apply also to other nanoparticle shapes and sizes. For an experimental demonstration, photoluminescence measurements with controlled emitter-particle surface distances would be necessary. Such a distance control has been successfully performed in recent works on the emission from purely electric dipole emitters.[7,11,20] Furthermore, it is essential to select a suitable emitter. The optical transition in question needs to have a sufficiently large magnetic component to demonstrate the effects that are predicted here for a purely magnetic dipole transition. This goal is achievable; for example, the magnetic component accounts for 77% of the intrinsic emission at 1548 nm in erbium-doped yttrium oxide.[56] Moreover, the emitter should be small enough as to serve as a probe with a sufficient spatial resolution. For example, Er^{3+} ions (size ∼ 0.1 nm) appear more suited than semiconductor quantum dots, whose size usually exceeds 1 nm.

The reduced emission quenching of MD transitions studied here may find promising applications in photoluminescence techniques: We expect that MD emitters can be positioned closer to metal surfaces than ED emitters without quenching the photoluminescence. For example, MD emitters could be adsorbed directly on metal surfaces and still radiate, if only their radiative centers are a minimum of ∼0.5 nm away from the surface; no spacer layers between emitters and metal surface would be necessary to prevent photoluminescence quenching. Similarly, surface-enhanced fluorescence from emitters in optical hot spots on nanostructured metal surfaces[57,58] might profit from the reduced quenching associated with MD emitters. Furthermore, the selective quenching of ED transitions in the sub-10 nm distance range might be usable to eliminate the ED contributions from the radiation emitted by mixed electric-magnetic dipole transitions such as those present in many transition-metal ions; this might lead to emission-modulation schemes similar in spirit to that demonstrated in ref 59. Moreover, the reduced quenching of MD transitions might also be useful for increasing the resolution of apertureless fluorescence microscopy using metallic scanning tips.[60]

In conclusion, we have demonstrated that the emission quenching of magnetic dipole transitions begins to dominate at substantially shorter distances to the surface of a metal nanoparticle than that of electric dipole transitions. We have explained this behavior in terms of the weaker distance dependence of the electric field induced by the magnetic dipole as compared to the electric field of an electric dipole. Our results imply that magnetic dipole transitions may be superior to electric ones whenever coupling to a metallic nanoantenna over sub-10 nm distances is used to enhance optical emission from a quantum emitter.

■ ASSOCIATED CONTENT

Supporting Information

The Supporting Information is available free of charge on the ACS Publications website at DOI: 10.1021/acsphotonics.5b00397.

Dielectric function of silver; decay rates of the electric-dipole transition; decay rates of the magnetic-dipole transition; quasi-static limit of the radiative rate; quasi-static limit of the nonradiative rate; emission quencing near an oblate spheroid; nonlocal corrections; supporting equations, figures, and references (PDF).

■ AUTHOR INFORMATION

Corresponding Author

*E-mail: chigrin@physik.rwth-aachen.de.

Notes

The authors declare no competing financial interest.

■ ACKNOWLEDGMENTS

We thank C. Rockstuhl, J. C. Goldschmidt, A. Pinchuck, T. Taubner, S. Fischer, F. Hallermann, and A. N. Sprafke for discussions. This work was supported by the Deutsche Forschungsgemeinschaft (DFG) through Project PI 261/5-1 and by the German Federal Ministry of Education and Research through the "Infravolt" Project (Contract Number 03SF0401E).

■ REFERENCES

(1) Maier, S. *Plasmonics: Fundamentals and Applications*; Springer, 2007.

(2) Stiles, P. L.; Dieringer, J. A.; Shah, N. C.; Van Duyne, R. R. Surface-Enhanced Raman Spectroscopy. *Annu. Rev. Anal. Chem.* **2008**, *1*, 601−626.

(3) Baker, G.; Moore, D. Progress in plasmonic engineering of surface-enhanced Raman-scattering substrates toward ultra-trace analysis. *Anal. Bioanal. Chem.* **2005**, *382*, 1751−1770.

(4) Jain, P. K.; Ghosh, D.; Baer, R.; Rabani, E.; Alivisatos, A. P. Near-field manipulation of spectroscopic selection rules on the nanoscale. *Proc. Natl. Acad. Sci. U. S. A.* **2012**, *109*, 8016−8019.

(5) Biagioni, P.; Huang, J.-S.; Hecht, B. Nanoantennas for visible and infrared radiation. *Rep. Prog. Phys.* **2012**, *75*, 024402.

(6) Fort, E.; Grésillon, S. Surface enhanced fluorescence. *J. Phys. D: Appl. Phys.* **2008**, *41*, 013001.

(7) Anger, P.; Bharadwaj, P.; Novotny, L. Enhancement and Quenching of Single-Molecule Fluorescence. *Phys. Rev. Lett.* **2006**, *96*, 113002.

(8) Bharadwaj, P.; Novotny, L. Spectral dependence of single molecule fluorescence enhancement. *Opt. Express* **2007**, *15*, 14266.

(9) Mertens, H.; Koenderink, A.; Polman, A. Plasmon-enhanced luminescence near noble-metal nanospheres: Comparison of exact theory and an improved Gersten and Nitzan model. *Phys. Rev. B: Condens. Matter Mater. Phys.* **2007**, *76*, 115123.

(10) Castanie, E.; Boffety, M.; Carminati, R. Fluorescence quenching by a metal nanoparticle in the extreme near-field regime. *Opt. Lett.* **2010**, *35*, 291−293.

(11) Reineck, P.; Gómez, D.; Ng, S. H.; Karg, M.; Bell, T.; Mulvaney, P.; Bach, U. Distance and Wavelength Dependent Quenching of Molecular Fluorescence by Au@SiO_2 Core-Shell Nanoparticles. *ACS Nano* **2013**, *7*, 6636−6648.

(12) Gersten, J. Spectroscopic properties of molecules interacting with small dielectric particles. *J. Chem. Phys.* **1981**, *75*, 1139.

(13) Dulkeith, E.; Morteani, A.; Niedereichholz, T.; Klar, T.; Feldmann, J.; Levi, S.; van Veggel, F.; Reinhoudt, D.; Möller, M.; Gittins, D. Fluorescence Quenching of Dye Molecules near Gold

DOI: 10.1021/acsphotonics.5b00397
ACS Photonics 2016, 3, 27−34

Nanoparticles: Radiative and Nonradiative Effects. *Phys. Rev. Lett.* **2002**, *89*, 203002.
(14) Gueroui, Z.; Libchaber, A. Single-Molecule Measurements of Gold-Quenched Quantum Dots. *Phys. Rev. Lett.* **2004**, *93*, 166108.
(15) Dulkeith, E.; Ringler, M.; Klar, T. A.; Feldmann, J.; Muñoz Javier, A.; Parak, W. J. Gold Nanoparticles Quench Fluorescence by Phase Induced Radiative Rate Suppression. *Nano Lett.* **2005**, *5*, 585−589.
(16) Schneider, G.; Decher, G.; Nerambourg, N.; Praho, R.; Werts, M. H. V.; Blanchard-Desce, M. Distance-Dependent Fluorescence Quenching on Gold Nanoparticles Ensheathed with Layer-by-Layer Assembled Polyelectrolytes. *Nano Lett.* **2006**, *6*, 530−536.
(17) Kühn, S.; HÅkanson, U.; Rogobete, L.; Sandoghdar, V. Enhancement of Single-Molecule Fluorescence Using a Gold Nanoparticle as an Optical Nanoantenna. *Phys. Rev. Lett.* **2006**, *97*, 017402.
(18) Bharadwaj, P.; Anger, P.; Novotny, L. Nanoplasmonic enhancement of single-molecule fluorescence. *Nanotechnology* **2007**, *18*, 044017.
(19) Vielma, J.; Leung, P. T. Nonlocal optical effects on the fluorescence and decay rates for admolecules at a metallic nanoparticle. *J. Chem. Phys.* **2007**, *126*, 194704.
(20) Pons, T.; Medintz, I. L.; Sapsford, K. E.; Higashiya, S.; Grimes, A. F.; English, D. S.; Mattoussi, H. On the quenching of semiconductor quantum dot photoluminescence by proximal gold nanoparticles. *Nano Lett.* **2007**, *7*, 3157−3164.
(21) Mertens, H.; Polman, A. Strong luminescence quantum-efficiency enhancement near prolate metal nanoparticles: Dipolar versus higher-order modes. *J. Appl. Phys.* **2009**, *105*, 044302.
(22) Pustovit, V. N.; Shahbazyan, T. V. Fluorescence quenching near small metal nanoparticles. *J. Chem. Phys.* **2012**, *136*, 204701.
(23) Huang, C.-C.; Chiang, C.-K.; Lin, Z.-H.; Lee, K.-H.; Chang, H.-T. Bioconjugated Gold Nanodots and Nanoparticles for Protein Assays Based on Photoluminescence Quenching. *Anal. Chem.* **2008**, *80*, 1497−1504.
(24) Novotny, L.; Hecht, B. *Principles of Nano-Optics*, 2nd ed.; Cambridge University Press, 2012; Cambridge Books Online.
(25) Stobbe, S.; Kristensen, P. T.; Mortensen, J. E.; Hvam, J. M.; Mørk, J.; Lodahl, P. Spontaneous emission from large quantum dots in nanostructures: Exciton-photon interaction beyond the dipole approximation. *Phys. Rev. B: Condens. Matter Mater. Phys.* **2012**, *86*, 085304.
(26) Kristensen, P. T.; Mortensen, J. E.; Lodahl, P.; Stobbe, S. Shell theorem for spontaneous emission. *Phys. Rev. B: Condens. Matter Mater. Phys.* **2013**, *88*, 205308.
(27) Thommen, Q.; Mandel, P. Left-handed properties of erbium-doped crystals. *Opt. Lett.* **2006**, *31*, 1803−1805.
(28) Dodson, C. M.; Zia, R. Magnetic dipole and electric quadrupole transitions in the trivalent lanthanide series: Calculated emission rates and oscillator strengths. *Phys. Rev. B: Condens. Matter Mater. Phys.* **2012**, *86*, 125102.
(29) Crosse, J.; Scheel, S. Atomic multipole relaxation rates near surfaces. *Phys. Rev. A: At., Mol., Opt. Phys.* **2009**, *79*, 062902.
(30) Taminiau, T. H.; Karaveli, S.; van Hulst, N. F.; Zia, R. Quantifying the magnetic nature of light emission. *Nat. Commun.* **2012**, *3*, 979−6.
(31) Schmidt, M. K.; Esteban, R.; Sáenz, J. J.; Suárez-Lacalle, I.; Mackowski, S.; Aizpurua, J. Dielectric antennas - a suitable platform for controlling magnetic dipolar emission. *Opt. Express* **2012**, *20*, 13636.
(32) Hein, S. M.; Giessen, H. Tailoring Magnetic Dipole Emission with Plasmonic Split-Ring Resonators. *Phys. Rev. Lett.* **2013**, *111*, 026803.
(33) Aigouy, L.; Cazé, A.; Gredin, P.; Mortier, M.; Carminati, R. Mapping and Quantifying Electric and Magnetic Dipole Luminescence at the Nanoscale. *Phys. Rev. Lett.* **2014**, *113*, 076101.
(34) Hussain, R.; Keene, D.; Noginova, N.; Durach, M. Spontaneous emission of electric and magnetic dipoles in the vicinity of thin and thick metal. *Opt. Express* **2014**, *22*, 7744.
(35) Zhao, Y.; Pan, H.; Lou, Y.; Qiu, X.; Zhu, J.; Burda, C. Plasmonic Cu2-xS Nanocrystals: Optical and Structural Properties of Copper-Deficient Copper(I) Sulfides. *J. Am. Chem. Soc.* **2009**, *131*, 4253−4261.
(36) Luther, J. M.; Jain, P. K.; Ewers, T.; Alivisatos, A. P. Localized surface plasmon resonances arising from free carriers in doped quantum dots. *Nat. Mater.* **2011**, *10*, 361−366.
(37) Rakic, A. D.; Djurišic, A. B.; Elazar, J. M.; Majewski, M. L. Optical Properties of Metallic Films for Vertical-Cavity Optoelectronic Devices. *Appl. Opt.* **1998**, *37*, 5271.
(38) Mortensen, N. A.; Raza, S.; Wubs, M.; Søndergaard, T.; Bozhevolnyi, S. I. A generalized non-local optical response theory for plasmonic nanostructures. *Nat. Commun.* **2014**,*5*.10.1038/ncomms4809
(39) Bohren, C. F.; Huffman, D. *Absorption and Scattering of Light by Small Particles*; Wiley Science Paperback Series; Wiley, 1983.
(40) Ruppin, R. Decay of an excited molecule near a small metal sphere. *J. Chem. Phys.* **1982**, *76*, 1681−1684.
(41) Klimov, V. V.; Letokhov, V. S. Electric and Magnetic Dipole Transitions of an Atom in the Presence of Spherical Dielectric Interface. *Laser Phys.* **2005**, *15*, 61−73.
(42) Schmidt, M. K.; Esteban, R.; Sáenz, J. J.; Suárez-Lacalle, I.; Mackowski, S.; Aizpurua, J. Dielectric antennas - a suitable platform for controlling magnetic dipolar emission: errata. *Opt. Express* **2012**, *20*, 18609.
(43) Colas des Francs, G.; Bouhelier, A.; Finot, E.; Weeber, J. C.; Dereux, A.; Girard, C.; Dujardin, E. Fluorescence relaxation in the near-field of a mesoscopic metallic particle: distance dependence and role of plasmon modes. *Opt. Express* **2008**, *16*, 17654.
(44) Xu, Y.; Lee, R.; Yariv, A. Quantum analysis and the classical analysis of spontaneous emission in a microcavity. *Phys. Rev. A: At., Mol., Opt. Phys.* **2000**, *61*, 033807.
(45) Asenjo-Garcia, A.; Manjavacas, A.; Myroshnychenko, V.; García de Abajo, F. J. Magnetic polarization in the optical absorption of metallic nanoparticles. *Opt. Express* **2012**, *20*, 28142.
(46) Chance, R. R.; Prock, A.; Silbey, R. Molecular Fluorescence and Energy Transfer Near Interfaces. *Advances in Chemical Physics*; John Wiley & Sons, 1978; Vol. *37*, pp 1−65.
(47) Joulain, K.; Carminati, R.; Mulet, J.-P.; Greffet, J.-J. Definition and measurement of the local density of electromagnetic states close to an interface. *Phys. Rev. B: Condens. Matter Mater. Phys.* **2003**, *68*, 245405.
(48) Suzuki, T.; Kawai, H.; Nasu, H.; Hughes, M.; Ohishi, Y.; Mizuno, S.; Ito, H.; Hasegawa, K. Quantum efficiency of Nd^{3+}-doped glasses under sunlight excitation. *Opt. Mater.* **2011**, *33*, 1952−1957.
(49) Ruppin, R. Optical Properties of a Plasma Sphere. *Phys. Rev. Lett.* **1973**, *31*, 1434−1437.
(50) Datsyuk, V. V.; Tovkach, O. M. Optical properties of a metal nanosphere with spatially dispersive permittivity. *J. Opt. Soc. Am. B* **2011**, *28*, 1224.
(51) David, C.; García de Abajo, F. J. Spatial Nonlocality in the Optical Response of Metal Nanoparticles. *J. Phys. Chem. C* **2011**, *115*, 19470−19475.
(52) Christensen, T.; Yan, W.; Raza, S.; Jauho, A.-P.; Mortensen, N. A.; Wubs, M. Nonlocal Response of Metallic Nanospheres Probed by Light, Electrons, and Atoms. *ACS Nano* **2014**, *8*, 1745−1758.
(53) Manjavacas, A.; García de Abajo, F. J.; Nordlander, P. Quantum Plexcitonics: Strongly Interacting Plasmons and Excitons. *Nano Lett.* **2011**, *11*, 2318−2323.
(54) Tame, M. S.; McEnery, K. R.; Özdemir, Ş. K.; Lee, J.; Maier, S. A.; Kim, M. S. Quantum plasmonics. *Nat. Phys.* **2013**, *9*, 329−340.
(55) Hajisalem, G.; Nezami, M. S.; Gordon, R. Probing the Quantum Tunneling Limit of Plasmonic Enhancement by Third Harmonic Generation. *Nano Lett.* **2014**, *14*, 6651−6654.
(56) Li, D.; Jiang, M.; Cueff, S.; Dodson, C. M.; Karaveli, S.; Zia, R. Quantifying and controlling the magnetic dipole contribution to 1.5 um light emission in erbium-doped yttrium oxide. *Phys. Rev. B: Condens. Matter Mater. Phys.* **2014**, *89*, 161409.
(57) Kinkhabwala, A.; Yu, Z.; Fan, S.; Avlasevich, Y.; Müllen, K.; Moerner, W. Large single-molecule fluorescence enhancements produced by a bowtie nanoantenna. *Nat. Photonics* **2009**, *3*, 654−657.

DOI: 10.1021/acsphotonics.5b00397
ACS Photonics 2016, 3, 27−34

(58) Cang, H.; Labno, A.; Lu, C.; Yin, X.; Liu, M.; Gladden, C.; Liu, Y.; Zhang, X. Probing the electromagnetic field of a 15-nanometre hotspot by single molecule imaging. *Nature* **2011**, *469*, 385−388.
(59) Karaveli, S.; Weinstein, A. J.; Zia, R. Direct Modulation of Lanthanide Emission at Sub-Lifetime Scales. *Nano Lett.* **2013**, *13*, 2264−2269.
(60) Azoulay, J.; Débarre, A.; Richard, A.; Tchénio, P. Quenching and enhancement of single-molecule fluorescence under metallic and dielectric tips. *EPL* **2000**, *51*, 374−380.

DOI: 10.1021/acsphotonics.5b00397
ACS Photonics 2016, 3, 27−34